BACKGROUND LIGHT ESTIMATION FOR DEPTH-DEPENDENT UNDERWATER IMAGE RESTORATION

Chau Yi Li, Andrea Cavallaro

Centre for Intelligent Sensing, Queen Mary University of London, UK

ABSTRACT

Light undergoes a wavelength-dependent attenuation and loses energy along its propagation path in water. In particular, the absorption of red wavelengths is greater than that of green and blue wavelengths in open ocean waters. This reduces the red intensity of the scene radiance reaching the camera and results in non-uniform light, known as background light, due to the scene depth. Restoration methods that compensate for this colour loss often assume constant background light and distort the colour of the water region(s). To address this problem, we propose a restoration method that compensates for the colour loss due to the scene-to-camera distance of non-water regions without altering the colour of pixels representing water. This restoration is achieved by ensuring background light candidates are selected from pixels representing water and then estimating the non-uniform background light without prior knowledge of the scene depth. Experimental results shows that the proposed approach outperforms existing methods in preserving the colour of water regions.

***Index Terms*—** Spectral distortion, restoration, underwater images, colour correction.

1. INTRODUCTION

Underwater images are important for a variety of applications, including marine species identification, underwater robot vision and navigation, and recreational photography [1]. The appearance of underwater objects is degraded by the combination of scattering and absorption of light, a phenomenon known as attenuation [2]. Attenuation is quantified by the attenuation coefficient, which depends on the composition of water and varies across geographic locations [3]. Scattering changes the direction of light propagation and contributes to blurring, whereas absorption reduces the light intensity along its propagation path. In open ocean waters, red light is absorbed to a greater extent than green and blue light [4], hence resulting in images with reduced red intensity, and blue or green colour cast.

The quality of underwater images can be improved using enhancement or restoration methods. Enhancement methods aim to remove the colour cast introduced by the vertical depth between the scene and water surface. Enhancement methods that employ global white-balancing to remove the colour cast [5, 6] often introduce artefacts in water regions. Restoration methods aim to compensate for the colour loss due to the scene-to-camera distance. In this paper we will focus on restoration methods.

Light attenuation can be modelled as an exponential decay. As such, light experiences a significant magnitude decrease in the first few meters underwater. This effect can be observed in images that capture a large vertical depth range, taken near the water surface or in water locations with large attenuation coefficients. While most underwater image processing methods assume constant global background light reaching the scene in an image, in these aforementioned cases, the assumption does not hold. Using a uniform global background light to recover the scene radiance leads to false colours in the water region. The only method that considers non-uniform background light requires knowledge of the scene depth-range and attenuation coefficients [7]. However, unless special devices are used, this information is generally not available.

In this paper, we propose a background light estimation algorithm that does not require prior knowledge of the scene depth or the attenuation coefficient. We considers the attenuation coefficients per unit *pixel distance* in the image, obtained by linear regression. We then interpolate the obtained coefficients to estimate the background light for the entire image. Unlike methods that use a uniform global background light, we use the estimated background light in the restoration. Using the estimated background light, we can reveal details of the scene that would otherwise be lost with a uniform global background light. Moreover, the proposed method avoids introducing artefacts in the water region.

2. BACKGROUND

Let $J(x, y)$ be the scene radiance at pixel location (x, y) and $t(x, y)$ be the transmission map, which modulates the portion of the scene radiance reaching the camera. The observed intensity, $I(x, y)$, can be described as [2]:

$$I(x, y) = t(x, y)J(x, y) + (1 - t(x, y))A, \tag{1}$$

where A is the global background light. The scene radiance, $J(x, y)$, can be recovered as:

$$J(x, y) = \frac{I(x, y)}{t(x, y)} - \frac{1 - t(x, y)}{t(x, y)}A. \tag{2}$$

As attenuation is wavelength dependent, $t(x, y)$ and A should be estimated accurately for each colour channel. While $t(x, y)$ determines the compensation extent for each pixel, A affects the overall brightness: being a subtractive term in Eq. (2), a brighter estimated A leads to a darker restored image. The effect is amplified when $t(x, y) < 0.5$. Selecting A from an appropriate region is therefore crucial to the quality of restored image.

Several underwater restoration methods [7, 8] use the dark channel prior [9], which was proposed for outdoor hazy images and shares the model in Eq. (1). The Dark Channel, $J^D(x, y)$, is defined by the minimum intensity value across the R, G, and B channels in a neighbourhood centred at (x, y). The dark channel prior states that $J^D(x, y) \to 0$ in a haze-free image. A is estimated as the brightest pixel from the top 0.1% of $J^D(x, y)$ pixels and is then used to normalise $J^D(x, y)$ to obtain $t(x, y)$. However, applying this prior to underwater images often results in selecting the red intensity chan-

Table 1: Comparison of methods for the estimations of the global background light, A, and the transmission map, $t(x, y)$. KEY – $J^D(x, y)$: Dark Channel; $J^R(x, y)$: Red Channel; β: attenuation coefficient; *Pro*: proposed method.

			[9]	[7]	[10]	[11]	*Pro*
A	prior	$J^D(x,y)$	✓	✓			
		$J^R(x,y)$			✓		
	constraint	blurriness				✓	
		variance				✓	✓
		ratio					✓
	estimate non-uniform A			✓			✓
t	fixed β			✓		✓	
	different t for each channel				✓	✓	✓
	t independent of A					✓	

nel as $J^D(x, y)$ and hence in *over-estimating* $t(x, y)$. Moreover, A is often picked from bright objects instead of from the water region, resulting in a darker restored image. The aforementioned problem can be addressed by considering light absorption (i.e. losses in the red channel) as the cue for $t(x, y)$. The Red Channel was proposed in [10] as

$$J^R(x, y) = \min_{(s,t)\in\Omega(x,y)} \{1 - I^r(s, t), I^g(s, t), I^b(s, t)\}, \quad (3)$$

for a neighbourhood $\Omega(x, y)$ centred at (x, y). The red channel prior states that $J^R(x, y) \to 0$ for objects close to the camera. A is selected as the pixel with the lowest red intensity from the top 10% brightest J^R pixels. However, not all objects contain red and therefore objects close to the camera, but with low red intensity, will be considered to be far away.

As light scattering causes blur in underwater images and the effect increases with the scene-to-camera distance, Gaussian filters can be applied to obtain a blurriness map as an indication of normalised distance [11]. The transmission map, $t(x, y)$, can be derived from the blurriness map using Eq. (4) with fixed attenuation coefficients and fixed distance range [11]. A is estimated as the weighted average of six candidate pixels selected from candidate regions obtained by successive quadtree subdivisions. This method fails to capture the distance of texture-less regions and the fixed distance range, when over-estimated, results in over-compensated colour.

The colour loss due to the vertical depth can be compensated using an estimation based on fixed attenuation coefficients and the dark channel prior [7]. After compensating for the scene-to-camera distance, the vertical depth is compensated with interpolated estimated background light. This is the only method that addresses the problem of non-uniform background light but with the assumption of known depth-range under water. However, fixed attenuation coefficients do not work across different geographic locations and the depth-range of the scene is generally unknown.

In summary, A is generally estimated from pixel candidates based on priors [7, 10], which are prone to noise, or from quadtree subdivisions, which obtain candidate regions based on statistical metrics [11, 12] and restricts the shape of candidate regions. Table 1 compares the restoration methods for estimating A and $t(x, y)$.

3. UNIFORM BACKGROUND LIGHT

In this section we present the derivation of global background light candidate regions, which is based on physical constraints that are valid in open ocean water. We also derive a transmission map that, when used for underwater image restoration, does not overcompensate for the red intensity channel.

According to the Beer-Lambert's Law [13], $t(x, y)$ can be represented as:

$$t(x, y) = e^{-\beta d(x,y)}, \quad (4)$$

where $d(x, y)$ is the scene-to-camera distance and β is the attenuation coefficient.

Let the attenuation coefficient and the global background light for red be β^r and A^r, respectively; and those for green or blue be β^c and A^c respectively, with $c \in \{g, b\}$. Similarly, let b^r and b^c be the scattering coefficient for red and for $c \in \{g, b\}$ respectively.

The ratio between attenuation coefficients can be expressed as [14]:

$$\frac{\beta^c}{\beta^r} = \frac{b^c A^r}{b^r A^c}, \quad (5)$$

and the ratio between scattering coefficients can be expressed as [3]:

$$\frac{b^c}{b^r} = \frac{a - b\lambda^c}{a - b\lambda^r}, \quad (6)$$

where $a = 1.62517$ and $b = 0.00113$.

As red light undergoes stronger attenuation than green and blue light, it follows that $\beta^r > \beta^c$. Moreover, consider the wavelength values $\lambda^r = 620nm$, $\lambda^g = 540nm$ and $\lambda^b = 450nm$ for red, green and blue light following [14], we can derive the following *ratio constraints* for global background light candidate:

$$\frac{A^r}{A^g} < 0.9109 \qquad and \qquad \frac{A^r}{A^b} < 0.8280. \quad (7)$$

The global background light should come from a flat intensity area. We therefore aim to ensure the uniformness of candidate regions, instead of the relative uniformness as done in other works that select the region with the lowest variance in successive quadtree subdivision [11]. To this end, we define the *variance constraint*, in which we calculate the variance, $\sigma^2(x, y)$, in a square window of size N centred at each (x, y) in the grayscale version of the input image. We only consider windows with sufficiently small variance: $\sigma^2(x, y) \leq \zeta^2$, with $\zeta = 0.01$ (i.e. 1% of the intensity range) and $N = 15$ for images whose size ranges from 300×400 to 720×1280.

The ratio and variance constraints defined above identify, respectively, pixel-wise and patch-wise candidates, which do not necessarily belong to the water region. To remove spurious candidates, we only consider region proposals with over 50% of pixels fulfilling both constraints as candidate regions, by combining the constraints with a bottom-up hierarchical segmentation, Multiscale Combinatorial Grouping [15]. Finally, the global background light, A, is chosen from candidate regions at pixel location

$$(x^*, y^*) = \arg\max_{(x,y)} \left(\max \left(I^g(x, y), I^b(x, y) \right) - I^r(x, y) \right). \quad (8)$$

The inner max operator selects the least attenuated colour channel among green and blue as the dominant channel for water. The pixel with the maximum difference between the dominating channel and the red channel, which is most attenuated, is selected to represent the scene at maximum distance from the camera.

As for the transmission map, we derive two partial maps with complementary information. First we obtain the texture map, which captures the scattering phenomenon as indication for transmission of *rich texture* regions. Similarly to [11], we capture this information using a Gaussian filter. To capture texture with different fineness, we use a Gaussian filter pyramid of 3 levels, each with 4 layers.

(a) (b)

Fig. 1: Example of preservation of the colour of the water region, while the colour loss of non-water regions is compensated for. (a) Original image; (b) restored scene radiance with uniform A.

(a) (b) (c)

Fig. 2: Impact of image depth-range compensation in the restoration process. (a) *Pro* (proposed method) with uniform A (note the pinkish top of the water region); (b) *Pro* with non-uniform A; (c) estimated non-uniform A.

Each filter has $\sigma_j^i = \sqrt{2^{i+j}}$, where i and j indexes level and layer respectively. The original image is input to the first level and the size is halved for each subsequent level. Each layer's output is the difference between the blurred and input image.

The texture map is the average of the output of all layers. However, as the histogram of this map skews to 0, we clip the values at the 95-th percentile to preserve the histogram characteristics while stretching the distribution to [0,1]. This map is unable to estimate the distance from the camera for regions with *plain texture* that, since there is no difference between the blurred and original image, will be considered far away from the camera.

The scene-to-camera distance can still be estimated based on the absorption of light, and hence the colour loss in the red channel. We obtain the Automatic Red Channel map M^R as proposed in [10]:

$$M^R(x) = 1 - \min\left\{ \frac{\min\limits_{y\in\Omega(x)} 1 - I^r(y)}{1 - A^r}, \frac{\min\limits_{y\in\Omega(x)} I^g(y)}{A^g}, \frac{\min\limits_{y\in\Omega(x)} I^b(y)}{A^b} \right\}. \tag{9}$$

The normalisation by A guarantees $M^R(x,y)$ to be in [0,1] and be comparable to the texture map, $M^{text}(x,y)$. Pure white and dark pixels contribute to $M^R(x,y)$ of 1, indicating minimum scene-to-camera distance. We combine the maps considering for each pixel location the transmission map value for red intensity channel, $\tilde{t}^r(x,y)$, to be the larger from the two partial maps: $\tilde{t}^r(x,y) = \max(M^{text}(x,y), M^R(x,y))$ and then refine $\tilde{t}^r(x,y)$ by soft matting [16].

The range of the above transmission map is in [0,1]. As small transmission values often lead to overcompensation for the red intensity channel, to avoid this effect we normalise the estimated transmission map to the range of $J^R(x,y)$ defined in Eq. (3). As such we no longer consider A, which has the smallest transmission map value, to be at infinite distance from the camera but at the same distance as the non-water scene that is farthest away from the camera.

With reference to Eq. (4), the transmission maps for green and blue, $t^c(x,y)$, can be obtained as

$$t^c(x,y) = t^r(x,y)^{\frac{\beta^c}{\beta^r}}, \tag{10}$$

where $\frac{\beta^c}{\beta^r}$ is obtained from Eq. (5) and is guaranteed to be < 1 by our *ratio constraint* for $\frac{A^r}{A^c}$. Hence for $t^r(x,y) \in [0,1]$, we have $t^r(x,y) \leq t^c(x,y)$ and equality holds only when $t^r(x,y) = 0$ or 1. This ensures that at the same pixel location, the red channel intensity is compensated to the same or greater extent than that of the other channels, as it is multiplied by a value that is not smaller. This respects the fact that in open ocean water red light loses its energy more quickly than green and blue, and hence shall be compensated to a greater extent.

After the estimation of $t(x,y)$ and A, we can restore the scene radiance using Eq. (2). An example is shown in Fig. 1. Fig. 2 shows that a uniform A introduces false colours in the water region if the background light is not uniform.

In the next section, we detail the proposed approach to estimate non-uniform background light and hence preserve the water colour.

4. IMAGE DEPTH-RANGE COMPENSATION

In this section we derive, without prior knowledge on the scene depth, the attenuation coefficient and background light that we will use to compensate for the image depth range.

Let us assume that natural light strikes the water surface evenly and the background light in the image is horizontally constant. The background light at the top of the image, A_0^c, undergoes attenuation for each vertical pixel distance D travelled. Our goal is to estimate the change of background light between two vertically adjacent pixels, quantified by the attenuation coefficient per pixel distance, $\hat{\beta}^c$.

The light intensity A_d^c at vertical pixel distance D from the top of the image can be calculated as

$$A_D^c = A_0^c e^{-\hat{\beta}^c D}, \tag{11}$$

which can also be written as $lnA_D^c = lnA_0^c - \hat{\beta}^c D$. We use linear regression to estimate lnA_0^c and $\hat{\beta}^c$. To this end, we select the column containing the global background light pixel, (x^*, y^*), from the corresponding connected component [1] of the global background light candidate regions, obtained in Sec. 3, and perform linear regression with L_1 error on the set $\{(x_i, ln\,(I\,(x_i, y^*)))\}$.

However, pairs of vertically adjacent pixels in the image may not represent the same vertical underwater depth when objects are captured at different distances from the camera. Let two pixels represent scene with distance D_0 and D_1 to the camera. The transmission map values for the corresponding points are $t_{D_0} = e^{-\beta D_0}$ and $t_{D_1} = e^{-\beta D_1}$ respectively. The ratio $D_0 : D_1$ can be calculated as $ln\,(t_{D_0}) : ln\,(t_{D_1})$ to obtain the scene-to-camera distances ratio between the concerned pixel and the estimated global background light pixel.

Finally, we obtain the background light for $c \in \{r,g,b\}$ as

$$A^c(x,y) = A^c \exp\left(-\hat{\beta}^c\,(x - x^*)\,\frac{ln\,(t^r\,(x,y))}{ln\,(t^r\,(x^*,y^*))}\right), \tag{12}$$

[1] To avoid the influence of lens distortion we do not consider the 5 pixels on the border of the image.

Table 2: Comparison of the methods under analysis. KEY – Org.: original image; ↑: the higher the better; ↓: the lower the better.

	Org.	DCP	ARC	WCID	BLA	*Pro*
$\text{MSE}_c \downarrow$	N/A	.0440	.0156	.0190	.0112	.0014
$\text{PSNR}_l \uparrow$	N/A	21.5	25.2	27.9	29.3	37.0
avg (%) ↑	9.9	15.8	9.5	16.9	30.9	16.9
UCIQE ↑	.5915	.6407	.5954	.6256	.6449	.6069

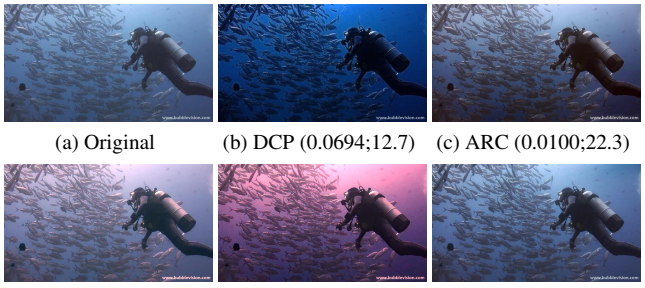

(a) Original (b) DCP (0.0694;12.7) (c) ARC (0.0100;22.3)

(d) WCID (0.0120;22.3) (e) BLA (0.0334;22.1) (f) *Pro* (0.0023;27.6)

Fig. 3: Example of preservation of water colour (scores represent MSE_c and PSNR_l respectively). Note that the proposed method reveals details at bottom of the image.

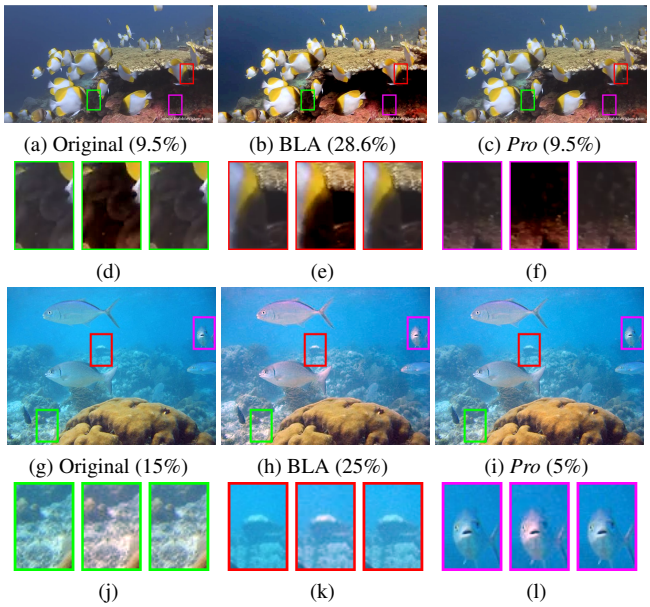

(a) Original (9.5%) (b) BLA (28.6%) (c) *Pro* (9.5%)

(d) (e) (f)

(g) Original (15%) (h) BLA (25%) (i) *Pro* (5%)

(j) (k) (l)

Fig. 4: Sample images (and corresponding subjective evaluation result). Patches in (d)-(f) and (j)-(l) are from Original; BLA; *Pro*.

where A^c is the estimated global background light and $t^r(x, y)$ is the estimated transmission map for the red intensity channel.

As linear regression is performed on the connected component containing the selected global background light, errors in global background light estimation algorithm can accumulate and affect the overall colour tone of the output image. To avoid error propagation, we impose the following constraint: if $\hat{\beta}^r < \hat{\beta}^{\{g,b\}}$ or $\hat{\beta}^c < 0$, then $\hat{\beta}^c = 0$, which reduces the background light to constant colour A. Then we recover the scene radiance with Eq. (2). An example of restoration using the estimated background light is shown in 2(b).

5. EXPERIMENTAL RESULTS

We compare the proposed method, *Pro*, with four other methods: Dark Channel Prior (DCP) [9], Automatic Red Channel (ARC) [10], Wavelength Compensation Image Dehazing (WCID) [7] and Blurriness and Light Absorption (BLA) [11]. We use a dataset of 60 images collected from three sources: [17][18][19]. We compare (i) the preservation of the water colour and (ii) the overall quality of the restored image. Results are summarised in Table 2.

To quantify the distortion of the water colour after restoration, we calculate the mean square error (MSE_c) across the R, G, and B channels and the peak-signal-to-noise ratio (PSNR_l) on the luminance channel between the original and restored images over pixels representing water, which we segmented with LabelMe [20]. For water colour preservation, *Pro* outperforms other methods by one order of magnitude. *Pro* achieves the lowest average MSE_c for the dataset (0.0014), followed by BLA (0.0112). ARC (0.0156) and WCID (0.0190) perform similarly, whereas DCP has a higher error (0.0440). *Pro* achieves the highest average PSNR_l (37.0), compared with the second highest obtained by BLA (29.3). Sample restored images are shown in Fig. 3.

We also asked viewers to compare the original and images restored with the five methods under analysis, and to select out of the six the most *attractive* image. Each image was evaluated at least 20 times and on average 20.25 times. The results (see Table 2, second-last row) are the average percentage of the method chosen by the observers. Note that the percentages may not add up to 1 due to rounding. In this small-scale evaluation, BLA obtains the highest score as it outputs high contrast images that are usually preferred by humans. However, images processed by BLA often include distorted water colour or unnatural appearance of scene (see Figs. 3 and 4). The images in Fig. 4(b)(h) were preferred to the images in (c)(i) (see subjective evaluation scores for each image). In Fig. 4(b), details are lost in BLA when the contrast is enhanced. In Fig. 4(h) the red channel is over-compensated so that the fish and the sand appear to be red.

Finally, although existing measures such as UCIQE [21] are biased towards images with certain characteristics that can also be due to undesirable distortions and are hence unreliable in predicting image quality [8], for completeness we also include, in the last row of Table 2, UCIQE values, which were generated with through PUIQE (`http://puiqe.eecs.qmul.ac.uk/`).

6. CONCLUSION

We proposed a restoration method for underwater images to compensate for colour distortions induced by the scene-to-camera distance. An important feature of the proposed method is that it compensates for the depth range without prior knowledge of the scene. The proposed method selects pixels representing water to estimate the global background light. Results show that the proposed method can restore the colour of non-water regions without distorting the water colour.

As future work, we aim to model scenes captured under artificial lights, as well as multiple reflections and blurring caused by suspended particles in turbid waters.

Acknowledgment. We used images from the PKU-EAQA dataset (which was collected under the sponsorship of the National Natural Science Foundation of China) and BubbleVision.

7. REFERENCES

[1] N. J. C. Strachan, "Recognition of fish species by colour and shape," in *J. Image Vis. Comput.*, Jan 1993.

[2] Y. Schechner and N. Karpel, "Clear underwater vision," in *Proc. IEEE CVPR*, Washington, DC, USA, Jul 2004.

[3] R. W. Gould, R. A. Arnone, and P. M. Martinolich, "Spectral dependence of the scattering coefficient in case 1 and case 2 waters," *Appl. Opt.*, vol. 38, no. 12, pp. 2377–2383, Apr 1999.

[4] S. Duntley, "Light in the sea," in *J. Opt. Soc. Amer.*, 1963, vol. 53, pp. 214–233.

[5] C. O. Ancuti, C. Ancuti, C. De Vleeschouwer, and P. Bekaert, "Color balance and fusion for underwater image enhancement," in *IEEE Trans. Image Process.*, Jan 2018, vol. 27, pp. 379–393.

[6] D. Berman, T. Treibitz, and S. Avidan, "Diving into haze-lines: Color restoration of underwater images," in *Proc. BMVC*, London, UK, 2017, BMVA Press.

[7] J. Chiang, Y. Chen, and Y. Chen, "Underwater image enhancement: Using wavelength compensation and image dehazing," in *IEEE Trans. Image Process.*, Apr 2012, vol. 21, pp. 1756–1769.

[8] S. Emberton, L. Chittka, and A. Cavallaro, "Underwater image and video dehazing with pure haze region segmentation," *Comput. Vis. Image Underst.*, pp. 1077–3142, Mar 2017.

[9] K. He, J. Sun, and X. Tang, "Single image haze removal using dark channel prior," in *IEEE Trans. Pattern Anal. Mach. Intell.*, Dec 2011, vol. 33, pp. 2341–2353.

[10] A. Galdran, D. Pardo, A. Picn, and A. Alvarez-Gila, "Automatic red-channel underwater image restoration," in *J. Vis. Commun. Image Represent.*, Jan 2015, vol. 26, pp. 132–145.

[11] Y. T. Peng and P. C. Cosman, "Underwater image restoration based on image blurriness and light absorption," in *IEEE Trans. Image Process.*, Apr 2017, vol. 26, pp. 1579–1594.

[12] C. Li, J. Guo, R. Cong, Y. Pang, and B. Wang, "Underwater image enhancement by dehazing with minimum information loss and histogram distribution prior," in *IEEE Trans. Image Process.*, Dec 2016, vol. 25, pp. 5664–5677.

[13] D. F. Swinehart, "The beer-lambert law," *J. Chem. Educ.*, p. 333, 1962.

[14] X. Zhao, T. Jin, and S. Qu, "Deriving inherent optical properties from background color and underwater image enhancement," in *J. Ocean Eng.*, Jan 2015, vol. 94, pp. 163–172.

[15] J. Pont-Tuset, P. Arbelaez, J. Barron, F. Marques, and J. Malik, "Multiscale combinatorial grouping for image segmentation and object proposal generation," in *IEEE Trans. Pattern Anal. Mach. Intell.*, Jan 2017, vol. 39, pp. 128–140.

[16] A. Levin, D. Lischinski, and Y. Weiss, "A closed form solution to natural image matting," in *IEEE Trans. Image Process.*, Feb 2007, vol. 30, pp. 228–242.

[17] BubbleVision, "Youtube," 2018, Available: https://www.youtube.com/user/bubblevision. [Accessed: 01- Feb- 2018].

[18] National Oceanic and Atmospheric Administration, "The noaa photo library," 2017, Available: http://www.photolib.noaa.gov [Accessed: 01- Sep- 2017].

[19] Z. Chen, T. Jiang, and Y. Tian, "Quality assessment for comparing image enhancement algorithms," in *Proc. IEEE CVPR*, Columbus, OH, USA, Jun 2014.

[20] B. C. Russell, A. Torralba, K. P. Murphy, and W. T. Freeman, "Labelme: a database and web-based tool for image annotation," in *Int. J. Comput. Vis.*, May 2008, vol. 77, pp. 157–173.

[21] M. Yang and A. Sowmya, "An underwater color image quality evaluation metric," in *IEEE Trans. Image Process.*, Dec 2015, vol. 24, pp. 6062–6071.